Stability mechanisms for plate-like nanoparticles immersed in a macroion dispersion

2009 J. Phys.: Condens. Matter 21 424107

(http://iopscience.iop.org/0953-8984/21/42/424107)

J. Phys.: Condens. Matter **21** (2009) 424107 (12pp) doi:10.1088/0953-8984/21/42/424107

Stability mechanisms for plate-like nanoparticles immersed in a macroion dispersion

Felipe Jiménez-Ángeles, Gerardo Odriozola and Marcelo Lozada-Cassou

Programa de Ingeniería Molecular, Instituto Mexicano del Petróleo, Lázaro Cárdenas 152, 07730 México, DF, Mexico

Received 30 April 2009, in final form 29 June 2009
Published 29 September 2009
Online at stacks.iop.org/JPhysCM/21/424107

Abstract

An integral equation theory and Monte Carlo simulations are applied to study a model macroion solution confined between two parallel plates immersed in a 1:1 electrolyte and the macroions' counterions. We analyze the cases in which plates are: (a) uncharged; (b) when they are like-charged to the macroions; (c) when they are oppositely charged to the macroions. For all cases a long range oscillatory behavior of the induced charge density between the plates is found (implying an overcompensation/undercompensation of the plates' charge density) and a correlation between the confined and outside fluids. The behavior of the force is discussed in terms of the macroion and ion structure inside and outside the plates. A good agreement is found between theoretical and simulation results.

(Some figures in this article are in colour only in the electronic version)

1. Introduction

Experiments have shown interesting phenomena associated with charged macroions in confinement: aqueous solutions of highly charged macroions confined between two like-charged parallel plates (with the macroions and the plates being similarly charged) induce an attraction between them [1]. Also, macroions exhibit attraction among themselves [2, 3] as well as transversal [1] and lateral [4] ordering. In a different kind of experiment, but in a sense similar to the previous ones, a mixture of DNA polyelectrolytes with cationic liposomes has been considered, giving rise to a multilamellar self-assembling of positively charged liposome membranes and intercalated negative DNA polyelectrolytes [5].

The interaction between two symmetrically charged parallel plates immersed in an electrolyte solution has been considered theoretically since the pioneering works of Derjaguin, Landau, Verwey and Overbeek (DLVO) [6, 7]. In their work, they solved the Poisson–Boltzmann equation for the electrical double layer (EDL) produced by an electrolyte confined between two parallel plates. The DLVO theory predicts an exponentially decaying repulsive interaction between the charged surfaces. Since Poisson–Boltzmann theory neglects ionic correlations, DLVO theory can be considered valid only for a restricted regime of conditions, i.e. low concentrated monovalent solutions and low electrostatic surface potentials. Later efforts to incorporate ionic short range correlations into the EDL have been made by means of integral equation theories [8–10], density functional theories [11–13] and computer simulations [9, 14, 15]. On the other hand, studies on the interaction force between two plate-like charged colloids have shown that multivalent electrolytes, at moderate and high concentrations, produce a non-monotonic decay which can turn attractive at certain separation distances [16–18]. Such non-monotonic and attractive behavior for the interaction between two like-charged cylindrical [19] and spherical [20] colloids has also been found.

Beyond the colloid–colloid interaction mediated by an electrolyte solution, interesting surface effects attributed to the proper consideration of ionic correlations have been predicted theoretically and corroborated by computer simulations, i.e. surface charge reversal [21–23], the reverse of macroion mobility [24–26], the non-monotonic relationship between the surface potential and surface charge density [23, 27], just to mention a few. Surface charge reversal refers to the surface charge overcompensation by an excess of oppositely charged particles adsorbed from the solution. This phenomenon has been observed for polyvalent and even for monovalent

ions [23, 28]. However, it is particularly magnified by polyelectrolytes and macroions [29–33], in which case this phenomenon is the basis for macroions self-assembling and polyelectrolyte complexation on surfaces [34, 35]. Macroion adsorption on colloid surfaces also provides innovative colloid stabilization mechanisms through the formation of halos [36]. Hence, the understanding of the EDL produced by complex charged fluids is recognized to be important in a broad variety of disciplines, from biology to physics. This has motivated theoretical and computer simulation efforts for describing macroion adsorption on charged surfaces (i.e. the EDL phenomenon produced by complex charged fluids, such as macroions, colloids and polyelectrolytes [29–33]). In this regard, in the past we applied an integral equation theory for inhomogeneous fluids to the EDL produced by a macroion solution next to a charged interface, where novel phenomena attributed to the consideration of size and electrostatic correlations have been described [30, 31]. Of particular interest are the results of overcharging [30] which implies the adsorption of ions onto a like-charged surface, and hence being different to charge reversal. Overcharging results from considering correlations among size-unsymmetrical charged species and has been observed in recent computer simulations [37]. It can also be predicted by Poisson–Boltzmann theories where macroion–macroion size correlations are neglected [38, 39].

By means of computer simulations, we recently studied the interaction between two like-charged plates in solution with two intercalated rod-like cylindrical macroions [40, 41]. In that work, we have found a plate–plate attractive interaction associated with entropic and electrostatic correlations induced by the presence of the charged rods. In the same way, we have shown that the presence of the plates dramatically reduces the rod–rod repulsion, turning it attractive at certain conditions, these findings being consistent with the experimental results of Rädler *et al* [5]. On the other hand, previous studies on the interaction between two charged parallel plates, with macroions at finite concentration in between, have been carried out by modeling macroion–macroion and surface–macroion through screened Coulomb potentials, predicting the macroions' ordering and the qualitative behavior for the plate–plate interaction [42–45]. However, these models do not consider correlations associated with the presence of counterions and electrolyte. Here we will show that the proper consideration of size and electrostatic correlations (due to macroions and small ions) reveal interesting phenomena in the behavior of the plate–plate effective interaction, concentration profiles and induced charge densities, and discuss the transversal and lateral ordering previously reported experimentally [1–4].

In this work we consider two like-charged (or uncharged) parallel plates immersed in a solution containing macroions, their counterions and an electrolyte. Hence, the electrostatic and size correlations originated by the presence of charge on the plates and the three charged species of the fluid are explicitly considered. The main purpose of this work is to study the effective interaction between the two like-charged (or uncharged) plates, the structure of the confined fluid and the adsorbed charge between the plates. Our studies are carried out by means of an integral equation theory and Monte Carlo computer simulations.

This paper is organized as follows: in section 2 we describe the integral equation method and the model for a macroion solution confined by two parallel charged plates as well as the simulation method. In the same section, we derive the *hypernetted chain/mean spherical* (HNC/MS) integral equations and the equations to compute the plate–plate effective interactions. In section 3 results are presented and discussed and, finally, in section 4 some conclusions are given.

2. Theory

2.1. Integral equations for inhomogeneous fluids

The method that we use to derive integral equations for inhomogeneous fluids makes use of a simple fact: an external field can be considered as a particle in the fluid, i.e. as one more species infinitely dilute. This statement is valid in general: however, it is particularly useful in the statistical mechanics theory for inhomogeneous fluids [46].

The multi-component Ornstein–Zernike equation for a fluid made up of $n+1$ species is

$$h_{ij}(\mathbf{r}_{21}) = c_{ij}(\mathbf{r}_{21}) + \sum_{m=1}^{n+1} \rho_m \int h_{im}(\mathbf{r}_{23}) c_{mj}(\mathbf{r}_{13})\, \mathrm{d}v_3, \quad (1)$$

where ρ_m is the number density of species m, $h_{ij}(\mathbf{r}_{21}) \equiv g_{ij}(\mathbf{r}_{21}) - 1$ and $c_{ij}(\mathbf{r}_{21})$ are the total and direct correlation functions for two particles at $\mathbf{r}_2$ and $\mathbf{r}_1$ of species i and j, respectively, with $g_{ij}(\mathbf{r}_{21})$ the pair distribution and $\mathbf{r}_{21} = \mathbf{r}_2 - \mathbf{r}_1$. Among the most well-known closures between $h_{ij}(\mathbf{r}_{21})$ and $c_{ij}(\mathbf{r}_{21})$ are [47]

$$c_{ij}(\mathbf{r}_{21}) = -\beta u_{ij}(\mathbf{r}_{21}) + h_{ij}(\mathbf{r}_{21}) - \ln g_{ij}(\mathbf{r}_{21}), \quad (2)$$

$$c_{ij}(\mathbf{r}_{21}) = -\beta u_{ij}(\mathbf{r}_{21}) \qquad \text{for } r_{21} \equiv |\mathbf{r}_{21}| \geqslant a_{ij}. \quad (3)$$

Equations (2) and (3) are known as the hypernetted chain (HNC) and the mean spherical (MS) approximations, respectively; $u_{ij}(\mathbf{r}_{21})$ is the direct interaction potential between two particles of species i and j, a_{ij} is their closest approach distance and $\beta \equiv 1/k_{\mathrm{B}}T$. Some more possibilities for solving equation (1) are originated by considering a closure for $c_{ij}(\mathbf{r}_{21})$ in the first term of equation (1) and a different one for $c_{mj}(\mathbf{r}_{13})$ in the second term of equation (1), giving rise to hybrid closures.

To derive integral equations for inhomogeneous fluids, we let an external field be one of the fluid species, say the $(n+1)$ species (hereinafter referred to as the γ species), which is required to be infinitely dilute, i.e. $\rho_\gamma \to 0$. Therefore, the total correlation function between the γ-species particle and a j-species particle is given by

$$h_{\gamma j}(\mathbf{r}_{21}) = c_{\gamma j}(\mathbf{r}_{21}) + \sum_{m=1}^{n} \rho_m \int h_{\gamma m}(\mathbf{r}_{23}) c_{mj}(\mathbf{r}_{13})\, \mathrm{d}v_3 \quad \text{with } j = 1, \ldots, n. \quad (4)$$

The total correlation functions for the remaining species satisfy a n-component Ornstein–Zernike equation as equation (1)

(with no γ species) from which $c_{mj}(\mathbf{r}_{13})$ is obtained. In this scheme, the pair correlation functions, $g_{\gamma j}(\mathbf{r}_{21})$, are just the inhomogeneous one-particle distribution functions, $g_j(\mathbf{r}_1)$, for particles of species j under the influence of an external field. Thus, $h_{\gamma j}(\mathbf{r}_{21})$ and $c_{\gamma j}(\mathbf{r}_{21})$ can be replaced by $h_j(\mathbf{r}_1) \equiv g_j(\mathbf{r}_1) - 1$ and $c_j(\mathbf{r}_1)$, respectively. Hence, the inhomogeneous local concentration for the j species is given by

$$\rho_j(\mathbf{r}_1) = \rho_j g_j(\mathbf{r}_1). \tag{5}$$

By using the HNC closure (equation (2)) for $c_{\gamma j}(\mathbf{r}_{21})$ in equation (4), we get

$$g_j(\mathbf{r}_1) = \exp\left\{-\beta u_j(\mathbf{r}_1) + \sum_{m=1}^{n} \rho_m \int h_m(\mathbf{r}_3) c_{mj}(\mathbf{r}_{13})\, \mathrm{d}v_3\right\}, \tag{6}$$

where the subindex γ has been omitted for consistency with equation (5). In our approach, $c_{mj}(\mathbf{r}_{13})$ in the integral of equation (6) is given by the direct correlation function for a n-component *homogeneous fluid*; that is, $c_{mj}(\mathbf{r}_{13})$ is obtained from equation (1) using one of the closures provided by equations (2) and (3). For the present derivation we will use $c_{mj}(\mathbf{r}_{13})$ obtained with the MS closure (equation (3)). Therefore, equation (6) becomes the hypernetted chain/mean spherical (HNC/MS) integral equations for an inhomogeneous fluid. This equation has shown to be particularly successful in the case of inhomogeneous charged fluids, providing a good agreement with molecular simulation data [23, 48].

2.2. Models

We considered two symmetric planar hard walls of thickness d, with a charge density σ on each surface, and separated by a distance τ between their inner surfaces (see figure 1). The fluid phase is made up in the following way: a two-component electrolyte plus a macroion species and their counterions. For simplicity the macroions' counterions are of the same species as the electrolyte. The three species are considered to be hard spheres of diameter a_i with a centered point charge $q_i = z_i e$ (z_i being the ionic valence, e the proton's charge and $i = +, -, \mathrm{M}$ standing for cations, anions and macroions, respectively). The solvent is considered as a uniform medium of dielectric constant ε. For simplicity, the plate's dielectric constant is equal to that of the solvent. In addition we set

$$a \equiv a_+ = a_- \leqslant a_\mathrm{M}. \tag{7}$$

Two ions of species m and j, with relative position r, interact via the following potential:

$$u_{mj}(r) = \begin{cases} \infty & \text{for } r < a_{mj}, \\ \dfrac{z_m z_j e^2}{\varepsilon r} & \text{for } r \geqslant a_{mj}, \end{cases} \tag{8}$$

with $m, j = +, -, \mathrm{M}$ and $a_{mj} \equiv (a_m + a_j)/2$.

The charge on each plate is compensated by an induced charge in the fluid, σ':

$$\sigma' \equiv \sigma^{\mathrm{in}} + \sigma^{\mathrm{out}} = -\sigma_T, \tag{9}$$

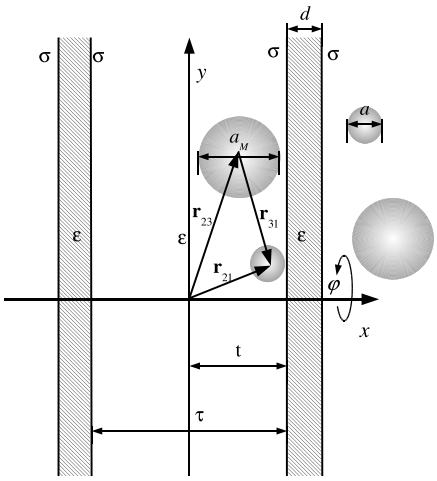

Figure 1. Schematic representation for a model macroion solution confined by a slit pore.

with $\sigma_T = 2\sigma$ and σ^{in} and σ^{out} being the induced charge between and outside the plates, respectively, which are given by

$$\sigma^{\mathrm{in}} = \int_0^t \rho_{\mathrm{el}}(x)\, \mathrm{d}x \tag{10}$$

and

$$\sigma^{\mathrm{out}} = \int_{t+d}^{\infty} \rho_{\mathrm{el}}(x)\, \mathrm{d}x, \tag{11}$$

where

$$\rho_{\mathrm{el}}(x) \equiv e \sum_{m=1}^{3} z_m \rho_m(x) \tag{12}$$

is the local charge density profile. By symmetry, similar expressions can be written for the left-hand side plate. Also we have used the fact that $(g_j(\mathbf{r}_1))$ depends only on the perpendicular distance to the plates, x, i.e. $g_j(\mathbf{r}_1) = g_j(x)$, and that the local concentration profile is $\rho_m(x) = \rho_m g_m(x)$. It should be pointed out that, in general, $-\sigma^{\mathrm{in}} \neq -\sigma^{\mathrm{out}} \neq \sigma$, i.e. there is a violation of the local electroneutrality condition [49–51].

According to the integral equation method outlined in section 2.1, the two parallel plates are considered as the γ species (see figure 1). The interaction potential between the plates and a j-species particle depends only on the particle position, x, referred to a Cartesian coordinate system with its origin located in the middle of the plates. Thus, we write $u_j(\mathbf{r}_1) = u_j(x)$, which is split as $u_j(x) = u_j^{\mathrm{el}}(x) + u_j^*(x)$, $u_j^{\mathrm{el}}(x)$ being the direct electrostatic potential and $u_j^*(x)$ the hard–core interaction. The former can be found from Gauss's law, i.e.

$$-\beta u_j^{\mathrm{el}}(x) = \frac{4\pi}{\varepsilon} z_j e \beta \sigma (2x + 2t + d + |x - t - d| + |x - t|). \tag{13}$$

The hard–core interaction is given by

$$u_j^*(x) = \begin{cases} \infty & \text{for } x \in [t - a_j/2, t + d + a_j/2] \\ 0 & \text{otherwise,} \end{cases} \tag{14}$$

for $j = +, -, \mathrm{M}$.

In the integral of equation (6) we use the MS expression of $c_{mj}(r_{13})$ for a primitive model *bulk* electrolyte, i.e.

$$c_{mj}(r_{13}) = \begin{cases} -\beta u^{\rm el}_{mj}(r_{13}) = -\beta \dfrac{z_m z_j e^2}{\varepsilon r} & \text{for } r_{13} \geqslant a_{mj}, \\ c^{\rm sr}_{mj}(r_{13}) + c^{\rm hs}_{mj}(r_{13}) & \text{for } r_{13} < a_{mj}, \end{cases} \tag{15}$$

where $r_{13} \equiv |\mathbf{r}_{13}|$ is the relative distance between two ions of species m and j. The particles short range correlations are considered through the *bulk* direct correlation functions $c^{\rm sr}_{mj}(r_{13})$ and $c^{\rm hs}_{mj}(r_{13})$. The explicit form of these functions is given in appendix A. Because of the system symmetry, it is convenient to use cylindrical coordinates in the integral of equation (6), and we can analytically integrate the ϕ and r coordinates (see figure 1), i.e. we consider a cylindrical coordinate system where $r_{13}^2 = x^2 + r^2 + y^2 - 2xy$ and $\mathrm{d}v_3 = \mathrm{d}\phi\, r\, \mathrm{d}r\, \mathrm{d}y$. After a lengthy algebra, from equation (6) we get [30, 31]

$$\begin{aligned} g_j(x) = \exp\Bigg\{ & -\beta u^{\rm el}_j(x) - 2\pi A_j(x) \\ & + 2\pi \sum_{m=1}^{3} \rho_m \int_D h_m(y) G_{mj}(x, y)\, \mathrm{d}y \\ & + 2\pi z_j \frac{e^2\beta}{\varepsilon} \sum_{m=1}^{3} z_m \rho_m \int_D h_m(y)[x + y + |x - y|]\, \mathrm{d}y \Bigg\} \end{aligned} \tag{16}$$

where we have defined

$$G_{mj}(x, y) = L_{mj}(x, y) + K_{mj}(x, y), \tag{17}$$

$$L_{mj}(x, y) = \int_{|x-y|}^{\infty} c^{\rm sr}_{mj}(r_{13}) r_{13}\, \mathrm{d}r_{13} = \frac{e^2\beta}{\varepsilon} D_{mj}(x, y), \tag{18}$$

$$K_{mj}(x, y) = \int_{|x-y|}^{\infty} c^{\rm hs}_{mj}(r_{13})\, r_{13}\, \mathrm{d}r_{13}, \tag{19}$$

and

$$\begin{aligned} A_j(x) = & \sum_{m=1}^{3} \rho_j \int_{t-a_m/2}^{t+d+a_m/2} G_{mj}(x, y)\, \mathrm{d}y \\ & + z_j z_3 \rho_3 \frac{\beta e^2}{\varepsilon} \int_{t+d+a/2}^{t+d+a_3/2} [x + y + |x - y|]\, \mathrm{d}y \\ & + z_j z_3 \rho_3 \frac{\beta e^2}{\varepsilon} \int_{t-a_3/2}^{t-a/2} [x + y + |x - y|]\, \mathrm{d}y. \end{aligned} \tag{20}$$

The expressions for the kernels, $K_{mj}(r, y)$ and $D_{mj}(x, y)$, are given in appendix B. Notice that in the integrals of equations (16) and (20), the fluid between the plates is correlated with the outside fluid.

2.3. The plates' effective interaction force

The derivation of the expression for the effective interaction force per unit area (P) between two charged plates immersed in a restricted primitive model electrolyte is given in detail elsewhere [16–18]. Hence, by following a similar procedure we obtain an identical expression when the plates are immersed in a three-species fluid, which can be written as

$$P = P_{\rm E} + P_{\rm C}. \tag{21}$$

where $P_{\rm E}$ is the electrostatic component given by

$$P_{\rm E} = -\frac{4\pi\sigma}{\varepsilon}(\sigma^{\rm out} - \sigma^{\rm in}) \tag{22}$$

$\sigma^{\rm in}$ and $\sigma^{\rm out}$ being the induced charge densities inside and outside the plates, respectively, given by equations (10) and (11). The contact component, $P_{\rm C}$, is written as

$$P_{\rm C} = k_{\rm B}T[\rho_0^{\rm in} - \rho_0^{\rm out}] \tag{23}$$

where $\rho_0^{\rm in}$ and $\rho_0^{\rm out}$ are the fluid total concentration at the inside and outside surfaces, respectively, which are expressed in terms of the contact value of the reduced concentration profiles as

$$\rho_0^{\rm in} = \sum_{i=1}^{3} \rho_i g_i(t - a_i/2), \tag{24}$$

and

$$\rho_0^{\rm out} = \sum_{i=1}^{3} \rho_i g_i(t + d + a_i/2). \tag{25}$$

The pressure in equation (21) is clearly the effective plate–plate interaction. Hence, for example, $P > 0$ implies an effective plate–plate repulsion.

2.4. Simulations

We employ Monte Carlo (MC) simulations for studying the system defined in section 2.2 and shown in figure 1. However, in this case the charge on the plates' surfaces is discretely assigned to points all having the unit of charge e. These charged points form a square grid on each plate surface, which are frequently and randomly moved in the x and y directions to mimic homogeneously charged surfaces. This is done for consistency with the integral equation theory calculations. The plates are inside a prism of sides $L_y = L_z = 175$ Å and $L_x = 350$ Å, which are much larger than the Debye–Hückel screening length for all studied cases. Additionally, L_z is larger than five times τ. These conditions are important to avoid box size effects. The origin of coordinates is set at the prism center. The 1–1 electrolyte is modeled by a restricted primitive model, i.e. by hard spheres of diameter a with a centered point charge, as well as the macroions which have a valence of $z_{\rm M}$ and a diameter of $5a$. For all cases, an electrolyte concentration of 0.1 M is set. These particles are initially randomly placed avoiding overlaps. Similar system set-ups were employed elsewhere to study forces between fixed macroparticles [19, 40].

In order to directly compare the MC simulations with the theoretical predictions, the excluded-volume interactions are modeled by hard potentials. That is, overlaps are always rejected and non-overlapping configurations are given an overall excluded-volume contribution of zero. On the other hand, the electrostatic contribution between any pair mj, where m and j are either grid charged sites of the plates and/or ions, is given by

$$U_{\rm el}(r) = k_{\rm B}T\ell_{\rm B}\frac{z_m z_j}{r_{mj}}, \tag{26}$$

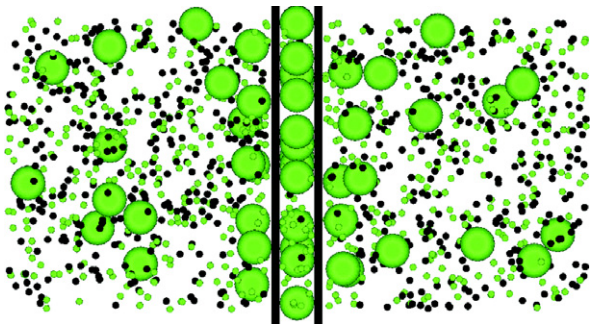

Figure 2. Snapshot of an equilibrated configuration for $\rho_M = 0.005$ M, $z_M = -5$, $\tau = 5.1a$ and $\sigma = 0.033$ C m^{-2}. Black and light (green online) particles correspond to positive and negative charges, respectively.

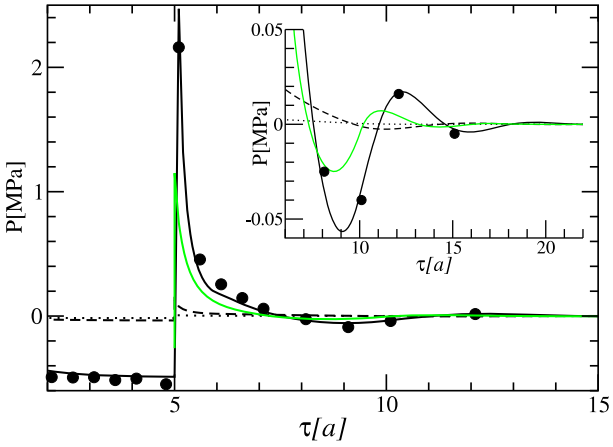

Figure 3. Total force per unit area between the two plates (P) as a function of their separation distance, τ. The plates are uncharged ($\sigma = 0$) and they are immersed in a solution containing macroions, their counterions and a 0.1 M monovalent electrolyte. (a) The dotted line corresponds to the HNC/MSA prediction for macroions at $\rho_M = 0.005$ M and $z_M = -5$ and (b) the dashed line corresponds to $\rho_M = 0.005$ M and $z_M = -15$. (c) The solid line and the black circles are, respectively, the HNC/MSA and MC simulation results for macroions at $\rho_M = 0.05$ M and $z_M = -5$. (d) The solid light curve (green online) is the result for uncharged macroparticles ($z_M = 0$) at $\rho_M = 0.05$ M. The inset shows a close up for $\tau \geqslant 6a$.

where r_{mj} is the distance between sites m and j, and z_m and z_j are the valences of sites m and j, respectively. The electrostatic strength is given by $\ell_B = \frac{e^2}{\varepsilon k_B T} = 7.14$ Å, the Bjerrum length. Electrostatic interactions were treated using the Ewald summation formalism. The convergence factor was fixed to $5.6/L_y$. There were set five reciprocal lattice vectors for y and z directions and six for x. In addition to the conventional MC trial moves, other ones having a maximum displacement of $L_y/2$ are done. This is necessary to access all of the configuration space volume, i.e. to allow ion interchange between the confined and unconfined regions. Both standard and large displacement trials are randomly called with equal probability. For the standard trials an acceptance probability of 0.4 was set, which corresponds to over 30 Å of cation and anion maximum displacements and a macroion maximum displacement close to 5 Å. The large displacement trials are accepted with probabilities close to 0.33 for cations and anions, and close to 5×10^{-4} for macroions. This is enough to produce a good sampling for 10^9 trials. Thus, there was no need to implement cluster moves [52], which will be surely necessary for macroions having larger surface charge density, larger size or for a lower temperature. A snapshot of an equilibrated configuration for $\rho_M = 0.005$ M, $z_M = -5$, $\tau = 5.1a$ and $\sigma = 0.033$ C m^{-2} is shown in figure 2.

The effective electrostatic force between plates is obtained by simply averaging all site contributions, i.e. by computing

$$\mathbf{F}_{el} = \left\langle \sum_m \sum_j -\nabla U_{el}(r_{mj}) \right\rangle, \tag{27}$$

where m runs over the sites of the reference plate and j runs over all other sites. The contact force contribution is obtained by integrating the ion contact density, i.e. by means of equations (23)–(25). In this case we approach the fluid total concentration at each side of the plates by extrapolating the concentration of each species close to the surfaces. Finally, it should be mentioned that these two contributions of the net force are interdependent.

3. Results and discussion

We have applied HNC/MSA theory and Monte Carlo simulations to study the effective interaction force between two like-charged (or uncharged) parallel plates, immersed in a fluid containing macroions, their counterions and an electrolyte. We also analyze the charge distribution inside and outside the plates through the reduced concentration profiles (RCP) and induced charge densities, σ^{in} and σ^{out}. For simplicity, we have considered the electrolyte to be size-symmetric (with an ionic diameter of $a_+ = a_- = a = 4.25$ Å), monovalent, and at a 0.1 M concentration. In all cases considered here, the macroions' diameter is $a_M = 5a = 21.25$ Å, the wall thickness is $d = a$ and the medium dielectric constant is $\varepsilon = 78.5$. We have considered several cases of macroion concentration, ρ_M, and valence, z_M, as well as the plates' surface charge density, σ. In all cases $z_M \leqslant 0$. Our results are organized according to the plate's surface charge density in the following order: first we present the results for uncharged plates, second for positive plates and, finally, for negative plates.

3.1. Uncharged plates

Figure 3 shows the HNC/MSA results for the plate–plate total interaction force per unit area, P, as a function of their separation distance (τ) for uncharged plates ($\sigma = 0$) and for three different macroion conditions: (a) $\rho_M = 0.005$ M and $z_M = -5$, (b) $\rho_M = 0.005$ M and $z_M = -15$, and (c) $\rho_M = 0.05$ M and $z_M = -5$; case (d) is for uncharged macroparticles ($z_M = 0$, $a_M = 5a$) at $\rho_M = 0.05$ M. We performed MC simulations only for case (c) and the results are included in the same plot, showing a good agreement with the corresponding results from HNC/MSA. In all cases, the interaction force between the uncharged plates is repulsive within the interval $5a < \tau \lesssim 7a$, oscillates between attraction and repulsion for $\tau \geqslant 7a$, and is attractive for $\tau < 5a$. This

repulsive interaction reaches its maximum as $\tau \to (5a)^+$, i.e. when there is just enough room to fit a macroion layer between the plates at $\tau \approx a_M$. The maximum of the interaction force is P^{max} equal to (a) 0.007 MPa, (b) 0.13 MPa, (c) 2.46 MPa and (d) 1.1 MPa, respectively, i.e. the repulsive interaction at $\tau \to (a_M)^+$ increases more importantly by increasing macroion concentration than by increasing their charge. This fact is better seen for uncharged macroparticles (d) which produce a value of P^{max} of the same order of magnitude as the charged ones at the same concentration (c), whereas those with a higher value of $|z_M|$ and lower concentration (b) are below by one order of magnitude. Actually, for $\rho_M = 0$, P is negligible for all τ (not shown). For $\tau > a_M$, P decreases as τ increases, reaching a minimum for certain plate–plate separation distances. The minimum is at $\tau \approx 9a$ for case (c) and at $\tau \approx 8.5a$ for case (d). Above this minimum, the force displays long range damped oscillations. For $\tau < a_M$, i.e. when macroions cannot penetrate between the plates, the interaction force abruptly turns negative and remains nearly constant as τ decreases up to $2a$. It should be mentioned that for this interval of τ the plates would collapse. However, the energetic barrier to reach this configuration is very high. This negative value of P is due to the pressure exerted by the outside macroions, which cannot be counterbalanced by the inside fluid since it does not contain macroions.

It should be noticed that both HNC/MSA and MC simulations show a discontinuity of P at $\tau = 5a = a_M$, occurring at crossover from $P > 0$ for $\tau \to (5a)^+$ to $P < 0$ for $\tau \to (5a)^-$. This is a signature of the transition from having macroions between the plates for $\tau \geqslant a_M$ to the absence of them for $\tau < a_M$. Apparently, the discontinuity of P is exclusive to this geometry since for two spherical or cylindrical colloidal particles there occurs only a discontinuity of the derivative of P [20, 53], i.e. $\lim_{\tau\to(a_M)^-} P' \neq \lim_{\tau\to(a_M)^+} P'$. These behaviors are related to the following facts: in planar geometry no particles are allowed to enter in between the pates, and abruptly a layer of them enters for surface–surface separation distances larger than the particles' size. In bispherical geometry, as the two spheres separate, they gradually leave space to finally allow a single particle to enter in between, and then the rest. The two-rod geometry shows an intermediate behavior between the planar and bispherical geometry, i.e. as the two rods separate a line of ions is allowed to be in between them [19].

Now we explain the behavior of $P(\tau)$ in terms of the reduced concentration profiles (see equations (21)–(25)). Figure 4 shows the HNC/MSA and MC simulation results for the RCP for macroions ($g_M(x)$), anions ($g_-(x)$) and cations ($g_+(x)$), and for three different plate–plate separation distances, i.e. $\tau = 12a$, $9a$ and $6a$. The HNC/MSA theory and MC simulations RCP show a good agreement. It is observed that the RCP at the outside of the plates remains nearly unchanged for the different values of τ, i.e. the three species are adsorbed on the surface (the RCP values at contact are greater than one, which is the bulk) and the RCP display damped oscillations as the distance to the outside surface increases, which are indicative of a transversal ordering of macroions near the wall. It should be pointed out that the

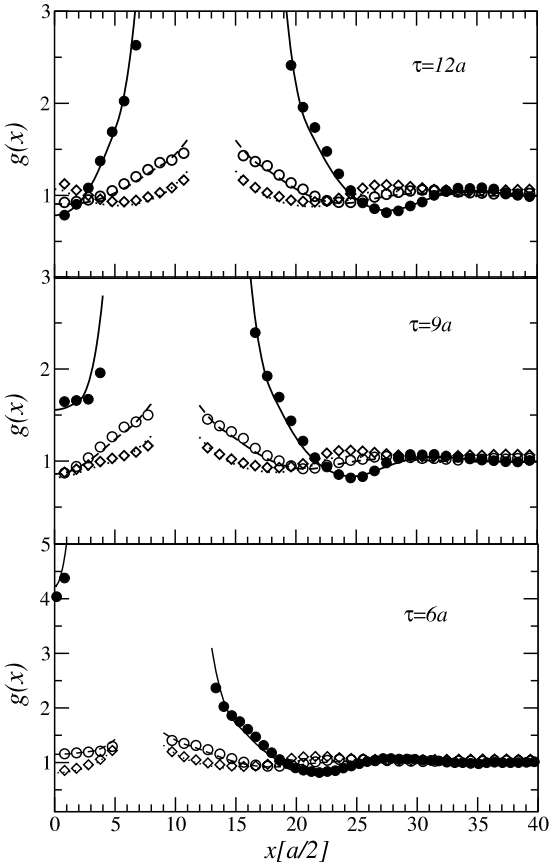

Figure 4. Reduced concentration profiles (RCP) from HNC/MSA for macroions ($g_M(x)$, solid line), anions ($g_-(x)$, dashed line) and cations ($g_+(x)$, dotted line) for three different plate–plate separation distances, i.e. $\tau = 12a$, $9a$ and $6a$. The black circles, white circles and white diamonds are, respectively, RCP from the MC simulations for macroions, anions and cations. The plates are uncharged ($\sigma = 0$) and are immersed in a solution containing macroions ($\rho_M = 0.05$ M, $z_M = -5$), their counterions and a 0.1 M monovalent electrolyte. The intervals where lines and symbols are interrupted correspond to the presence of the plate.

adsorption of particles towards the uncharged plates' surfaces is driven by the need of the system for releasing space, i.e. for increasing entropy [30]. Hence, the damped oscillations of the macroions' RCP reflect in a lesser degree the same need of the system to increase entropy. The maxima and minima remain located at the same distance to the outer surface. Even the contact value of the macroions' RCP at the outside surface, $g_M(\tau/2+d+a_M/2)$, remains constant as a function of τ, except for $\tau \to (a_M)^+$, where it slightly decreases (not shown). This is due to the macroion–macroion correlation across the plates. On the other hand, the RCP at the interplate region strongly change with τ. In particular, the behavior of the confined macroions is different from that for the outside macroions at plate–plate separation distances of a few macroions' diameters. Notice that the inside macroion contact value is nearly equal to that of the outside macroions for $\tau = 12a$, is lower for $\tau = 9a$ and higher for $\tau = 6a$. The inside macroions' local concentration increases as $\tau \to (a_M)^+$, which implies an effective decrease of their mutual repulsion, induced by the presence of the plates: this decrease in the effective macroion–

macroion repulsion is a consequence of the energy–entropy balance in the system, i.e. while the macroion–macroion electrostatic and hard-sphere forces are always repulsive, the many-body effective force has an attractive contribution due to the need of the system for optimizing available space. The interrelation of these attractive and repulsive forces can be seen in equation (16), which is a many-body expression of the Leibniz energy balance approach, equivalent to Newton's force balance approach. Although not shown, MC simulations display a higher lateral ordering of the confined macroions than those adsorbed at the outside surfaces. For $\tau < a_M$ the macroions leave completely the inside region of the plates, which implies an attractive plate–plate interaction force. It should be mentioned that the RCP are just plotted for positive values of x, since they are symmetrical around $x = 0$.

For $\tau = 12a$, a nearly symmetric behavior of the inside and outside RCP can be seen as a function of the distance to the plate surface, which is slightly broken by the higher contact value of the inside macroions' RCP with respect to the outside contact value. This gives rise to a small plate–plate repulsive effective interaction force (see the inset of figure 3). As τ decreases slightly below $\tau = 2a_M = 10a$, the macroions adsorbed on the two inner sides of the plates strongly interact, hence promoting the release of macroions from the inside. This release of macroions increases the accessible volume inside the pore and thus enlarges the macroions' concentration at the pore center (see figure 4 for $\tau = 9a$). The combination of macroion release and the increase of their concentrations at the pore center give rise to a desorption from the pore surface, which in turn produces an attractive plate–plate effective interaction force. Finally, for $\tau \to a_M^+$, i.e. when there is space to nearly accommodate macroions in a single layer, there is an increase of macroion concentration at the plates' middle plane and at their surfaces (see figure 4 for $\tau = 6a$). This macroion layer enhances the plate–plate repulsive interaction force as $\tau \to a_M^+$.

Behind the adsorption of macroions on the plates' surfaces is the need of the system to increase the available volume, i.e. the increase of entropy. Hence, the uneven adsorption at both sides of the plates produces an attractive force and, on the other hand, the charge on the macroions produces a repulsive interaction. The balance of these two forces, one of entropic origin and the other of electrostatic energy origin, leads to regions of plate–plate mechanical equilibrium (see figure 3). This entropy energy balance between two uncharged plate-like nanoparticles and the macroions is an explanation for the colloidal stabilization by nanoparticle halos reported by Tohver *et al* [36].

3.2. *Positively charged plates*

We now discuss the results when the plates and macroions are oppositely charged.

Figure 5 shows the HNC/MSA and MC simulation results for the plate–plate total interaction force per unit area, P, and its electrostatic (P_E) and contact (P_C) components, as a function of their separation distance (τ). For reference we included the plate–plate interaction force in the absence of macroions ($\rho_M = 0$) at the same values of the surface charge density and electrolyte concentration. The plates are positively charged ($\sigma = 0.033$ C m^{-2}) and are immersed in a macroion solution at $\rho_M = 0.05$ M and with $z_M = -5$ plus a 0.1 M electrolyte. We wish to point out the similarities and differences between P for this case and for $\sigma = 0$: there is an induced repulsive interaction maximum at $\tau \to (a_M)^+$, which is induced by the presence of macroions. However, in this case it is almost five times higher than for the uncharged case since the number of macroions between the plates increases due to the charge on the plates. In both cases, for $\tau > a_M$, P decreases as τ increases and reaches a minimum at about $\tau \approx 6a$. Above this minimum, the force displays damped oscillations. The location of the minimum occurs at a smaller value of τ than for the uncharged plates. In the same way as for the uncharged plates, at $\tau = a_M$ the force is discontinuous and turns negative for $\tau \lesssim a_M$. However, in this case it displays a monotonically increasing behavior as τ decreases and eventually becomes positive at plate–plate separation distances of a few ionic diameters. This negative value of P at $\tau \lesssim a_M$ is due to the unbalanced pressure exerted by the outside macroions, and at small values of τ it is counterbalanced by the unscreened electrostatic repulsive force between the plates. As for the uncharged plates, in this case a good agreement between HNC/MSA and MC results is found for the three curves. We wish to highlight that the main contribution to the plate–plate repulsive interaction (P) is provided by a contact component (P_C). Finally, it should be mentioned that the force between the plates in the absence of macroions shows a completely different behavior, i.e. $P(\tau)$ is always positive and monotonically decreasing as τ increases.

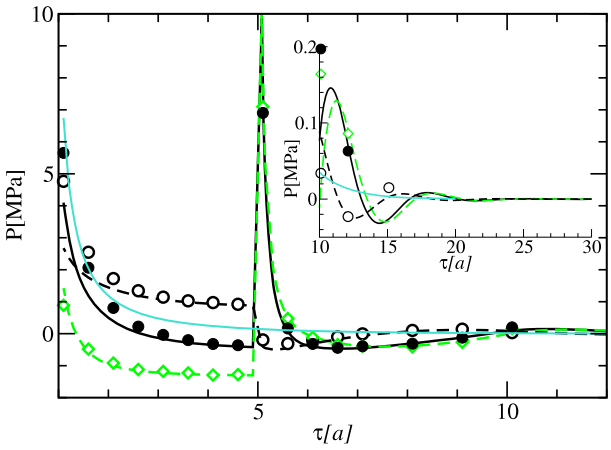

Figure 5. Total force per unit area between the two plates (P) and its contact (P_C) and electrostatic (P_E) components, as a function of their separation distance, τ. The black solid, light dashed (green online), and black dashed lines are, respectively, the HNC/MSA results for P, P_C and P_E, whereas the black circles, light open diamonds (green online) and white circles correspond to the MC simulation results. The plates are positively charged ($\sigma = 0.033$ C m^{-2}) and are immersed in a solution containing macroions ($\rho_M = 0.05$ M and $z_M = -5$), their counterions and a 0.1 M monovalent electrolyte. The solid light curve (blue online) is the total interaction force when there are no macroions but only a monovalent 0.1 M electrolyte for the same plate surface charge density. The inset shows a close up for $\tau \geqslant 10a$.

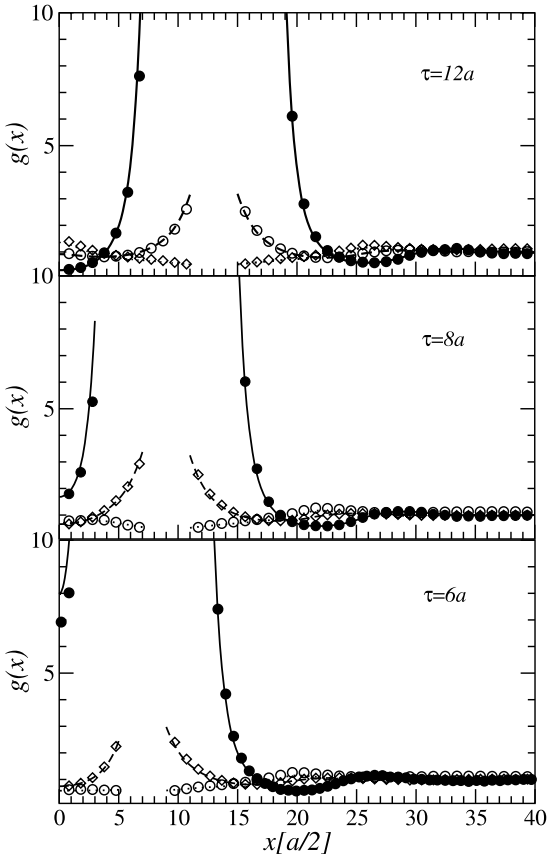

Figure 6. Reduced concentration profiles (RCP) from HNC/MSA for macroions ($g_{\mathrm{M}}(x)$, solid line), anions ($g_{-}(x)$, dashed line) and cations ($g_{+}(x)$, dotted line) for three different plate–plate separation distances, i.e. $\tau = 12a$, $8a$ and $6a$. The black circles, white circles and white diamonds are, respectively, RCP from the MC simulations for macroions, anions and cations. The plates are positively charged ($\sigma = 0.033$ C m^{-2}) and are immersed in a solution containing macroions ($\rho_{\mathrm{M}} = 0.05$ M, $z_{\mathrm{M}} = -5$), their counterions and a 0.1 M monovalent electrolyte.

Figure 6 shows the RCP from HNC/MSA and MC simulations for macroions ($g_{\mathrm{M}}(x)$), anions ($g_{-}(x)$) and cations ($g_{+}(x)$), and for three different plate–plate separation distances, i.e. $\tau = 12a$, $8a$ and $6a$. As for the uncharged plates, in general, the results from HNC/MSA theory show a good agreement with those from MC simulations. It is seen that the RCP at the outside of the plates remain nearly unchanged for the different values of τ, i.e. the macroions and anions are adsorbed towards the surface whereas cations are expelled from it. Also, the RCP display damped oscillations as the distance to the outside surface increases. These oscillations of the outside RCP remain unaltered for the different values of τ. Actually, the oscillations of the RCP for macroions and anions are similar to those for $\sigma = 0$, but for this case the macroion adsorption is enhanced due to the charge on the plate surfaces. This implies that the transversal ordering induced by the presence of the plates does not change its wavelength as compared to that in the uncharged plates' case. However, due to the higher macroion adsorption, in the charged case, a higher lateral macroion ordering is observed, owing to the less space available. Thus, the confined macroions display higher lateral

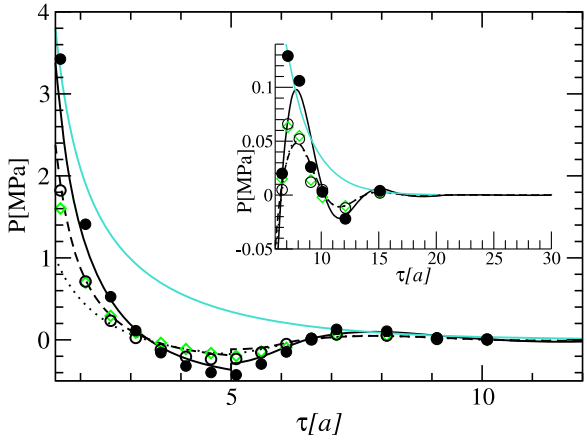

Figure 7. Total force per unit area between the two plates (P) and its contact (P_{C}) and electrostatic (P_{E}) components, as a function of their separation distance, τ. The solid, dashed and dotted lines are, respectively, the HNC/MSA results for P, P_{C} and P_{E}, whereas the black circles, white circles and open diamonds (green online) correspond to the MC simulation results. The plates are negatively charged ($\sigma = -0.033$ C m^{-2}) and are immersed in a solution containing macroions ($\rho_{\mathrm{M}} = 0.05$ M and $z_{\mathrm{M}} = -5$), their counterions and a 0.1 M monovalent electrolyte. The solid light curve (blue online) is the total interaction force when there are no macroions but only a monovalent 0.1 M electrolyte for the same plate surface charge density. The inset shows a close up for $\tau \geqslant 10a$.

ordering than those at the outside surfaces since their local concentration is higher inside than outside. Hence, as for the uncharged plates, for $\tau = 12a$, a nearly symmetric behavior of the inside and outside RCP is seen as a function of the distance to the plate surface. This symmetry is broken by the higher contact value of the inside macroions' RCP with respect to the outside contact value. This gives rise to a plate–plate repulsive effective interaction force. As discussed for the uncharged plates' case, as τ decreases slightly below $\tau = 2a_{\mathrm{M}} = 10a$, the macroions adsorbed at the inner surfaces strongly interact, promoting their release (see figure 6 for $\tau = 8a$). The combination of macroion release and their desorption from the pore surface produces an attractive plate–plate effective interaction force. Finally, for $\tau \to a_{\mathrm{M}}^{+}$, i.e. when there is space to nearly accommodate macroions in a single layer, there is an increase of macroion concentration at the pore's and at the plates' surface (see figure 6 for $\tau = 6a$). This macroion layer originates an abrupt increase of the plate–plate repulsive interaction force as $\tau \to a_{\mathrm{M}}^{+}$.

3.3. Negatively charged plates

In this case, macroions and plates are like-charged and thus they play the role of coions. The pressure on the plates (P) and its components (P_{C} and P_{E}), for this case, are shown in figure 7 as a function of τ for ($\sigma = -0.033$ C m^{-2}), $\rho_{\mathrm{M}} = 0.05$ M and $z_{\mathrm{M}} = -5$. In the same plot, the pressure when no macroions are considered is included, i.e. by only accounting for the monovalent electrolyte at $\rho_{\mathrm{M}} = 0.1$ M. Mainly, the non-monotonic behavior of P as a function of τ in the presence of macroions is noted, showing several attractive regions. As in positive and uncharged plates, this oscillatory behavior is

long ranged, only disappearing for $\tau > 20a$ (see the inset of figure 7). This is completely different from the monotonic behavior of P obtained for pure electrolyte. This is surprising at first sight, since naively one would expect coions to have a small influence on the surface interaction. For this case, however, macroions adopt interesting configurations between the plates that give rise to the non-monotonic behavior of P. It is interesting to note that both the electrostatic P_E and contact P_C components contribute with the same sign to P, for all τ. In particular both curves are practically overlapping for $\tau \gtrsim 3a$, and below this point the contact component dominates. The small discontinuity of P and P_C for $\tau = a_M$ should be noted, owing to the presence and absence of macroions between the plates.

The behavior of P can be explained in terms of the RCP of the different species at different separation distances, τ. These are shown for $\tau = 15a$, $10a$ and $8a$ in figure 8. There, contrary to the results for positive and uncharged plates, it is shown that macroions are not directly adsorbed by the plate surfaces. That is, the value for the macroions' RCP at contact is close to zero for all cases. However, there is an adsorption of macroions at a second layer mediated by the adsorbed cations. A maximum of the macroions' RCP for large plate–plate separation distances is seen, i.e. at a distance of approximately $7a$ from the inner and outer surfaces ($x \approx \pm 6(a/2)$ and $x \approx \pm 26(a/2)$, for $\tau = 15a$). This adsorption of macroions on a like-charged surface is probably related to the observed halos of charged nanoparticles around microparticles reported by Tohver *et al* [36]. In their work, they studied a suspension of nearly uncharged microparticles plus like-charged nanoparticles. Hence, it is interesting to note that our results for uncharged or charged plates immersed in a like-charged macroion solution both predict a plate–plate stabilization mechanism. As the two plates approach, the two maxima of the RCP for macroions inside the pore, at both sizes of the plane of symmetry at $x = 0$, collapse into a single one at $x = 0$ from about $\tau = 2a_M$. This implies the formation of a single layer of macroions at the plates' middle plane, which increase their local concentration at $x = 0$ (hence increase their lateral ordering and decrease their mutual repulsion) as $\tau \to a_M^+$. This mechanism is different to that for positive and uncharged plates, where a layer is adsorbed on each surface and a single layer is obtained only as $\tau \to a_M$. In this case, the most adsorbed species are the small cations. Thus, their adsorption, influenced by the presence of macroions, mostly explains the behavior of the plate–plate entropic (contact) pressure. The case of $\tau = 15a$ corresponds to the situation where P is slightly positive, caused by a higher adsorption of cations inside the pore than outside. For $\tau = 10a$, P and its components P_E and P_C are nearly zero, implying a balance between the inner and outer fluids. For the case $\tau = 8a$, there is a larger adsorption of cations inside the plates, thus explaining the positive P value found at this distance. The negative values of P for $3a_M < \tau < 9a_M$ has to do with the release of macroions from the inside of the plates which are surrounded by their neutralizing cations. However, the release of cations from the inside continues for $\tau < a_M$ since some of them remained between the plates, overcompensating the inner surface charge density. By decreasing τ below $3a$ the higher confinement prompts a higher cation adsorption onto the plates' inner surface, hence giving rise to a higher contribution from the inside fluid on P_C, turning P positive. In short, the interaction force between the plates for the case in which the plates and macroions are like-charged can be understood in terms of the adsorption of macroion–small ion complexes onto the plates' surfaces.

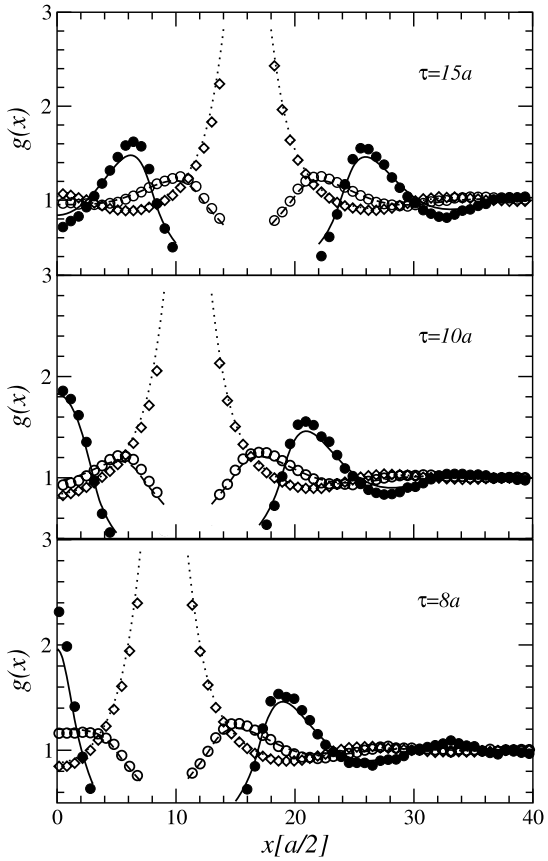

Figure 8. Reduced concentration profiles (RCP) from HNC/MSA for macroions ($g_M(x)$, solid line), anions ($g_-(x)$, dashed line) and cations ($g_+(x)$, dotted line) for three different plate–plate separation distances, i.e. $\tau = 15a$, $10a$ and $8a$. The black circles, white circles and white diamonds are, respectively, RCP from the MC simulations for macroions, anions and cations. The plates are negatively charged ($\sigma = -0.033$ C m^{-2}) and are immersed in a solution containing macroions ($\rho_M = 0.05$ M, $z_M = -5$), their counterions and a 0.1 M monovalent electrolyte.

3.4. Induced charge densities

Figure 9 shows the HNC/MSA and MC simulation results for the excess charge density between the plates, defined as $\sigma + \sigma^{in}$, as a function of τ for uncharged ($\sigma = 0$), positive ($\sigma = 0.033$ C m^{-2}) and negative ($\sigma = -0.033$ C m^{-2}) plates, immersed in a macroion solution ($\rho_M = 0.05$ M, $z_M = -5$). It should be pointed out that the overall electroneutrality condition is always satisfied, that is, the plates' charge density is compensated by an induced charge density inside (σ^{in}) and outside (σ^{out}) the plates, so that $\sigma^{in} + \sigma^{out} = -2\sigma$. The fact that $\sigma + \sigma^{in}$ goes to zero as $\tau \to \infty$ implies that the local

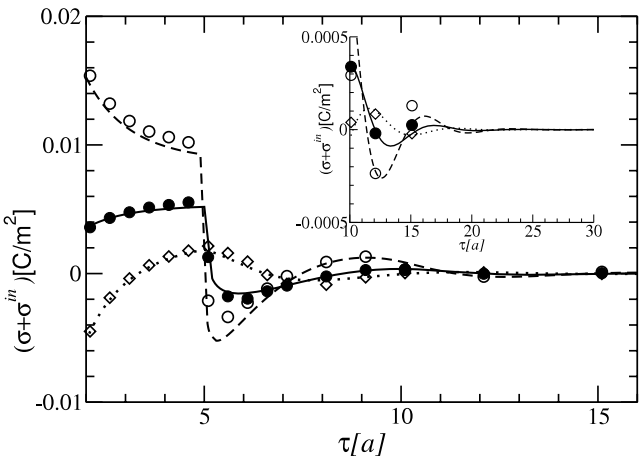

Figure 9. Excess charge density between the plates, $\sigma + \sigma^{\text{in}}$, as a function of their separation distance, τ. The plates are immersed in a solution containing macroions ($\rho_{\text{M}} = 0.05$ M, $z_{\text{M}} = -5$), their counterions and a 0.1 M monovalent electrolyte. The three different curves correspond to the HNC/MSA results for $\sigma = 0$ (solid line), $\sigma = 0.033$ C m^{-2} (dashed line) and $\sigma = -0.033$ C m^{-2} (dotted line), whereas the black circles, white circles and white diamonds are, respectively, the results from MC simulations. The inset shows a close up for $\tau \geqslant 10a$.

electroneutrality condition is satisfied for large plate–plate separation distances, i.e. the induced charge density at each side of the plate compensates the charge of its corresponding surface. On the other hand, for $\tau < a_{\text{M}} = 5a$, $\sigma^{\text{in}} + \sigma > 0$ for $\sigma = 0$ and for 0.033 C m^{-2}, owing to the excess of macroions adsorbed at the outside of the plates. For $\sigma = -0.033$ C m^{-2}, $\sigma^{\text{in}} + \sigma$ is positive for $3a \lesssim \tau < 5a$, since macroions are expelled from inside the plates. For the three cases shown here, as τ increases above $a_{\text{M}} = 5a$, $\sigma^{\text{in}} + \sigma$ displays a damped oscillatory behavior between positive and negative values, being of higher intensity for the positive plates, followed by the uncharged ones and of less intensity for the negative plates. The negative intervals of $\sigma^{\text{in}} + \sigma$ correspond to an overcompensation of σ^{in} by the adsorbed macroions, whereas the positive ones have to do with their expulsion from the inside. We see that, in all cases, the most dramatic reduction of macroion adsorption occurs as $\tau \to (a_{\text{M}})^{+}$, i.e. when there is just enough room to accommodate a single macroion layer between the plates. It is interesting to note that negative values of $\sigma^{\text{in}} + \sigma$, within $6a \lesssim \tau \lesssim 10a$ for $\sigma = -0.033$ C m^{-2}, are due to the increase of macroion concentration at the plates' middle plane (see the maximum in their RCP at $x = 0$ in figure 8). The adsorption of macroions between the plates is a consequence of the need of the system for releasing space, i.e. for increasing entropy, which is maximized when macroions are adsorbed inside or outside the plates. According to this principle, the adsorption of macroions is favored over the small ions since they release more space. Hence, the intervals of negative charge are produced when more macroions are adsorbed than the necessary small ions to compensate their charge, reflecting the prevalence of the space optimization over the neutrality condition.

4. Conclusions

The effective interaction force between two parallel plates immersed in a macroions plus electrolyte solution was studied by means of an integral equation theory and Monte Carlo simulations. In all cases, i.e. when the plates were uncharged, and when the macroions and the plates were like-charged and oppositely charged, an oscillatory behavior of the force, between attraction and repulsion, was found. Hence the presence of macroions originates several plate–plate distances of mechanical equilibrium. In particular, we wish to highlight that, when the plates are uncharged or like-charged to the macroions, this mechanical equilibrium is associated with the adsorption of macroions onto the plates' surface. We believe this mechanism is related to the observed colloid stabilization mechanisms induced by the formation of nanoparticle halos around microparticles [36]. Also, a long range oscillatory behavior of the induced charge density between the plates is observed, implying an overcompensation/undercompensation of the plates' charge density and a correlation between the confined and outside fluids. In addition, our MC results show a transversal ordering of the adsorbed macroions. Both oscillatory behaviors can be explained in terms of the energy–entropy balance, where the electrostatic and hard-sphere repulsive forces are in competition with the effective attractive force, due to the need of the system to optimize the available space, i.e. of increasing entropy.

To the best of our knowledge, this paper exhibits the first comparison between HNC/MSA theory and simulations for an electrical double-layer system with macroions at finite concentration. In general, a quantitatively good agreement is found between them, pointing out that the HNC/MSA theory properly captures electrostatic and short range correlations of all species.

Acknowledgment

We dedicate this work to the memory of our friend and colleague Yurko Duda.

Appendix A. The mean spherical closure

The primitive model is the simplest model for an electrolyte that includes some of the most relevant aspects of real solutions. In the general case the primitive model is constituted by n species of particles embedded in a uniform medium of dielectric constant ε at temperature T. Each species is defined by the particles' point charge at the center, $q_i = z_i e$ (where e stands for the proton's charge and z_i for the ionic valence), the ionic diameter, a_i, and number concentration, ρ_i. The fluid is constrained to the following condition:

$$\sum_{i=1}^{n} z_i \rho_i = 0. \tag{A.1}$$

The expressions for the direct correlation functions, $c_{ij}(r_{13})$, for a *bulk* electrolyte (required in equation (6)) were

obtained by Blum [54] and Hiroike [55], through the MS closure, and are written as

$$c_{ij}(r_{13}) = \frac{e^2\beta}{\varepsilon} d_{ij}(r_{13}) + c_{ij}^{\rm hs}(r_{13}) - \beta\frac{z_i z_j e^2}{\varepsilon r_{13}}, \tag{A.2}$$

with $c_{ij}^{\rm sr}(r_{13}) = \frac{e^2\beta}{\varepsilon} d_{ij}(r_{13})$, $\beta = 1/k_{\rm B}T$ and

$$d_{ij}(r_{13}) = \begin{cases} b_{ij}^{(1)} + \dfrac{z_i z_j}{r_{13}}, & \text{for } 0 \leqslant r_{13} \leqslant \lambda_{ij}, \\ \dfrac{b_{ij}^{(2)} + z_i z_j}{r_{13}} - b_{ij}^{(3)} + b_{ij}^{(4)} r_{13} + b_{ij}^{(5)} r_{13}^3, & \\ \quad \text{for } \lambda_{ij} < r_{13} \leqslant a_{ij}, & \\ 0, \quad \text{for } r_{13} > a_{ij}; & \end{cases} \tag{A.3}$$

with $\lambda_{ij} \equiv \frac{|a_i - a_j|}{2}$ and $a_{ij} \equiv \frac{a_i + a_j}{2}$. The constants in equation (A.3) are given by

$$s_i = (n_i + \Gamma x_i),$$

$$b_{ij}^{(1)} = 2\left[z_i n_j - x_i s_i + \frac{a_i}{3} s_i^2\right],$$

$$b_{ij}^{(2)} = (a_i - a_j)\left\{\frac{(x_i + x_j)}{4}[s_i - s_j] - \frac{(a_i - a_j)}{16}[(n_i + \Gamma x_i + n_j + \Gamma x_j)^2 - 4 n_i n_j]\right\},$$

$$b_{ij}^{(3)} = (x_i - x_j)(n_i - n_j) + (x_i^2 + x_j^2)\Gamma + (a_i + a_j) n_i n_j - \tfrac{1}{3}[a_i s_i^2 + a_j s_j^2],$$

$$b_{ij}^{(4)} = \frac{x_i}{a_i} s_i + \frac{x_j}{a_j} s_j + n_i n_j - \frac{1}{2}[s_i^2 + s_j^2],$$

$$b_{ij}^{(5)} = \frac{s_j}{6a_j^2} + \frac{s_i}{6a_i^2},$$

where x_i are defined as $x_i \equiv z_i + n_i a_i$ and Γ is obtained from the solution of the following algebraic equation:

$$\Gamma^2 = \frac{\pi e^2 \beta}{\varepsilon} \sum_{i=1}^{n} \rho_i (z_i + n_i a_i)^2. \tag{A.4}$$

The n_i are obtained from the solution of the following set of algebraic equations:

$$-(z_i + n_i a_i)\Gamma = n_i + c a_i \sum_{j=1}^{n} (z_i + n_j a_i), \tag{A.5}$$

where $c = \frac{\pi}{2}[1 - \frac{\pi}{6}\sum_{j=1}^{n} \rho_i a_i^3]^{-1}$.

Considering that $a = a_1 = a_2$, $c_{ij}^{\rm hs}(r_{13})$ is just the direct correlation function for a hard-sphere *binary* mixture in the PY approximation. For particles of the same size it is given by [56]

$$c_{ii}^{\rm hs}(r_{13}) = \begin{cases} -A_i - B_i r_{13} - \delta r_{13}^3 & \text{for } r_{13} < a_i, \\ 0, & \text{for } r_{13} > a_i \end{cases} \tag{A.6}$$

For particles of different sizes we have

$$c_{13}^{\rm hs}(r_{13}) = \begin{cases} -A_1 \quad \text{for } s \leqslant \lambda_{13}, \\ -A_1 - \dfrac{[\alpha x^2 + 4\lambda_{13}\delta x^3 + \delta x^4]}{r_{13}} \\ \quad \text{for } \lambda_{13} < r_{13} \leqslant a_{13}, \\ 0 \quad \text{for } r_{13} > a_{13} \end{cases} \tag{A.7}$$

with $x \equiv r_{13} - \lambda_{13}$. The constants used in equations (A.6) and (A.7) are given by

$$A_1 = (1 - \eta_T)^{-3}\left\{1 + \eta_T + \eta_T^2 + \frac{\pi}{6} a^3 \rho_T [1 + 2\eta_T] - \frac{\pi}{2}\rho_3 (a_3 - a)^2 \{a(1 + \eta_3) + a_3[1 + 2(\eta_1 + \eta_2)]\}\right\} + \frac{\pi a^3}{2}(1 - \eta_T)^{-4}\left\{\rho_T(1 + \eta_T + \eta_T^2) - \frac{\pi}{2}\rho_3(\rho_1 + \rho_2)(a_3 - a)^2\left[(a + a_3) + a a_3 \frac{\pi}{6}\sum_{i=1}^{3}\rho_i a_i^2\right]\right\}, \tag{A.8}$$

$$\alpha = -\pi a_{13} g_{13}(a_{13}) \sum_{i=1}^{3} \rho_i a_i g_{ii}(a_i), \tag{A.9}$$

$$\delta = \frac{\pi}{12}\sum_{i=1}^{3}\rho_i A_i, \tag{A.10}$$

$$B_1 = B_2 = -\pi[(\rho_1 + \rho_2) a^2 g_{11}^2(a) + \rho_3 a_3 g_{13}^2(a_{13})], \tag{A.11}$$

with

$$g_{11}(a) = g_{22}(a) = \{[1 + \tfrac{1}{2}\eta_T] + \tfrac{3}{2}\eta_3 a_3^3 (a - a_3)\}(1 - \eta_T)^{-2},$$
$$g_{13}(a_{13}) = \frac{[a_3 g_{11}(a) + a g_{33}(a_3)]}{2a_{13}}. \tag{A.12}$$

The expressions for A_3, B_3 and $g_{33}(a_3)$ are obtained by interchanging $\eta_1 + \eta_2$, $\rho_1 + \rho_2$ and a_1 with η_3, ρ_3 and a_3, respectively, in the expressions for $A_1 B_1$, $g_{11}(a)$.

Appendix B. The kernel expressions

Carrying out the integrations indicated in equations (18) and (19), using equations (A.3), (A.6) and (A.7), the expressions for $K_{ij}(x, y)$ and $D_{ij}(x, y)$ are

$$D_{ij}(x, y) = \begin{cases} b_{ij}^{(1)} k_0 + z_i z_j J_1 + b_{ij}^{(2)} M_1 - b_{ij}^{(3)} M_2 + b_{ij}^{(4)} M_3 + b_{ij}^{(5)} M_5, & \\ \quad \text{for } 0 \leqslant |x - y| \leqslant \lambda_{ij}, & \\ (b_{ij}^{(2)} + z_i z_j) J_1 - b_{ij}^{(3)} J_2 + b_{ij}^{(4)} J_3 + b_{ij}^{(5)} J_5, & \text{for } \lambda_{ij} < |x - y| \leqslant a_{ij}, \\ 0, \quad \text{for } a_{ij} < |x - y| & \end{cases} \tag{B.1}$$

$$-K_{ii}(x, y) = \begin{cases} A_i J_2 + B_i J_3 + \delta J_5, & \text{for } a_{ii} \geqslant |x - y|, \\ 0, & \text{for } a_{ii} < |x - y|, \end{cases} \tag{B.2}$$

$$-K_{13}(x, y) = \begin{cases} A_1 J_2 + \alpha a^3/3 + \delta\lambda_{13} a^4 + \delta a^5/5, & \\ \quad \text{for } |x - y| < \lambda_{13}, & \\ A_1 J_2 + \upsilon P_3 + 4\delta\lambda_{13} P_4 + \delta P_5, & \\ \quad \text{for } \lambda_{13} < |x - y| \leqslant a_{13}, & \\ 0, \quad \text{for } a_{13} < |x - y|, & \end{cases} \tag{B.3}$$

where we use the following definitions:

$$J_n = (a_{ij}^n - |x - y|^n)/n, \tag{B.4}$$

$$P_n = (a^n - (|x - y| - \lambda_{ij})^n)/n, \tag{B.5}$$

$$M_n = (a_{ij}^n - \lambda_{ij}^n)/n, \tag{B.6}$$

and

$$k_0 = (\lambda_{ij}^2 - (x - y)^2)/2. \tag{B.7}$$

References

[1] Tulpar A, van Tassel P R and Waltz J 2006 *Langmuir* **22** 2876
[2] Crocker J C and Grier D 1996 *Phys. Rev. Lett.* **77** 1897
[3] Kepler G M and Fraden S 1994 *Phys. Rev. Lett.* **73** 356
[4] Larsen A E and Grier D G 1997 *Nature* **385** 230
[5] Rädler J O, Koltover I, Salditt T and Safinya C R 1997 *Science* **275** 810
[6] Verwey E J and Overbeek J T G 1948 *Theory of the Stability of Lyophobic Colloids* (Amsterdam: Elsevier)
[7] Derjaguin B V and Landau L 1941 *Acta Physicochim. (USSR)* **14** 633
[8] Lozada-Cassou M 1981 *J. Chem. Phys.* **75** 1412
[9] Lozada-Cassou M, Saavedra-Barrera R and Henderson D 1982 *J. Chem. Phys.* **77** 5150
[10] Kjellander R 1988 *J. Chem. Phys.* **88** 7129
[11] Mier y Teran L, Suh S H, White H S and Davis H T 1990 *J. Chem. Phys.* **92** 5087
[12] Patra C N and Ghosh S K 1994 *J. Chem. Phys.* **100** 5219
[13] Yu Y-X, Wu J and Gao G-H 2004 *J. Chem. Phys.* **120** 7223
[14] Torrie G M and Valleau J P 1980 *J. Chem. Phys.* **73** 5807
[15] Caillol J M and Levesque D 1991 *J. Chem. Phys.* **94** 597
[16] Lozada-Cassou M 1984 *J. Chem. Phys.* **80** 3344
[17] Lozada-Cassou M and Díaz-Herrera E 1990 *J. Chem. Phys.* **92** 1194
[18] Lozada-Cassou M and Díaz-Herrera E 1990 *J. Chem. Phys.* **93** 1386
[19] Jiménez-Ángeles F, Odriozola G and Lozada-Cassou M 2006 *J. Chem. Phys.* **124** 134902
[20] Allahyarov E and Löwen H 2001 *Phys. Rev.* E **63** 041403
[21] Greberg H and Kjellander R 1998 *J. Chem. Phys.* **7** 2940
[22] Attard P 1996 *Advances in Chemical Physics* vol XCII (New York: Wiley)
[23] Deserno M, Jiménez-Ángeles F, Holm C and Lozada-Cassou M 2001 *J. Phys. Chem.* B **105** 10983
[24] Lozada-Cassou M, González-Tovar E and Olivares W 1999 *Phys. Rev.* E **60** R17
[25] Lozada-Cassou M and González-Tovar E 2002 *J. Colloid Interface Sci.* **239** 285
[26] Tanaka M 2004 *J. Phys.: Condens. Matter* **16** S2127
[27] González-Tovar E, Jiménez-Ángeles F, Messina R and Lozada-Cassou M 2003 *J. Chem. Phys.* **120** 9782
[28] Messina R, González-Tovar E, Lozada-Cassou M and Holm C 2002 *Europhys. Lett.* **60** 383
[29] Tanaka M and Grosberg A Y 2001 *J. Chem. Phys.* **115** 567
[30] Jiménez-Ángeles F and Lozada-Cassou M 2004 *J. Phys. Chem.* B **108** 7286
[31] Jiménez-Ángeles F and Lozada-Cassou M 2004 *J. Phys. Chem.* B **108** 1719
[32] Terao T and Nakayama T 2002 *Phys. Rev.* E **65** 021405
[33] Messina R 2009 *J. Phys.: Condens. Matter* **21** 113102
[34] Decher G 1997 *Science* **277** 1232
[35] Caruso F, Caruso R A and Möhwald H 1998 *Science* **282** 1111
[36] Tohver V, Smay J E, Braun P V and Lewis J A 2001 *Proc. Natl Acad. Sci.* **98** 8950
[37] Chialvo A A and Simonson J M 2008 *J. Phys. Chem.* C **112** 19521
[38] Yu J, Aguilar-Pineda G E, Antillón A, Dong S-H and Lozada-Cassou M 2006 *J. Colloid Interface Sci.* **295** 124
[39] Messina R 2007 *J. Chem. Phys.* **127** 214901
[40] Odriozola G, Jiménez-Ángeles F and Lozada-Cassou M 2006 *Phys. Rev. Lett.* **97** 018102
[41] Odriozola G, Jiménez-Ángeles F and Lozada-Cassou M 2006 *J. Phys.: Condens. Matter* **18** S2335
[42] González-Mozuelos P, Alejandre J and Medina-Noyola M 1991 *J. Chem. Phys.* **95** 8337
[43] Kim Y-W, Kim S-C and Suh S-H 1999 *J. Chem. Phys.* **110** 1230
[44] Choudhury N and Ghosh S K 1996 *J. Chem. Phys.* **104** 9563
[45] Trokhymchuk A, Henderson D, Nikolov A and Wasan D T 2005 *Langmuir* **21** 10240
[46] Lozada-Cassou M 1993 *Fundamentals of Inhomogeneous Fluids* ed D Henderson (New York: Dekker) chapter 8
[47] Hansen J P and Mcdonald I R 1986 *Theory of Simple Liquids* 2nd edn (London: Academic)
[48] Lozada-Cassou M, Olivares W and Sulbarán B 1996 *Phys. Rev.* E **53** 522
[49] Lozada-Cassou M and Yu J 1996 *Phys. Rev. Lett.* **77** 4019
[50] Lozada-Cassou M and Yu J 1997 *Phys. Rev.* E **56** 2958
[51] Aguilar G E, Lozada-Cassou M and Yu J 2002 *J. Colloid Interface Sci.* **254** 141
[52] Orkoulas G and Panagiotopoulos A Z 1994 *J. Chem. Phys.* **101** 1452
[53] Jiménez-ángeles F, Messina R, Holm C and Lozada-Cassou M 2003 *J. Chem. Phys.* **119** 4842
[54] Blum L 1975 *Mol. Phys.* **30** 1529
[55] Kazuo H 1977 *Mol. Phys.* **33** 1195
[56] Lebowitz J L 1964 *Phys. Rev.* **133** A895